J Mol Model (2013) 19:4887–4895
DOI 10.1007/s00894-013-1992-8

ORIGINAL PAPER

Discovery of σ-hole interactions involving ylides

Jiannan Ji · Yanli Zeng · Xueying Zhang · Shijun Zheng · Lingpeng Meng

Received: 12 July 2013 / Accepted: 29 August 2013 / Published online: 17 September 2013

Abstract The positive electrostatic potentials (σ-hole) have been found in ylides CH_2XH_3 (X = P, As, Sb) and CH_2YH_2 (Y = S, Se, Te), on the outer surfaces of group VA and VIA atoms, approximately along the extensions of the C–X and C–Y bonds, respectively. These electrostatic potentials suggest that the above ylides can interact with nucleophiles to form weak, directional noncovalent interactions similar to halogen bonding interactions. MP2 calculations have confirmed the formation of CH_2XH_3···HM complexes (X = P, As, Sb; M = BeH, ZnH, MgH, Li, Na). The interaction energies, interaction distances, topological properties (electron density and its Laplacian), and energy properties (kinetic electron energy density and potential electron energy density) at the X(1)···H(10) bond critical points are all correlated with the most negative electrostatic potential value of HM, indicating that electrostatic interactions play an important role in these weak X···H interactions. Similar to the halogen bonding interactions, weak interactions involving ylides may be significant in several areas such as organic synthesis, crystal engineering, and design of new materials.

Keywords Electrostatic potential · Halogen bond · σ-hole interaction · Ylide

Introduction

Noncovalent interactions play a critical role in chemistry, biology and physics [1–3], especially in supramolecular chemistry [4–7], as molecular assemblies are usually held together through weak interactions. Interest in new types of intermolecular interactions, such as σ-hole [8–15] and π-hole [15, 16] interactions has recently grown.

The "σ-hole" refers to the outer region of depleted electronic density and positive electrostatic potential Vs(r) along the extension of the σ-type bond to atom X (X = group IV–VII atom) [8, 9]. The formation of σ-hole interactions are formed by a σ-hole and a negative electrostatic potential site B, with the R-X···B angle close to 180°. For example, the halogen bonding can be explained as the electrostatic interaction between the positive electrostatic potential region (σ-hole) and negative sites, resulting in an interaction angle of nearly 180°. Halogen, chalogen, pnicogen and group IV interactions are all under the umbrella of sigma-hole interactions, instead of following a tendency to view these as separate types of interactions [17–19].

Studies have demonstrated that a variety of condensed-phase physical properties dependent upon noncovalent interactions can be expressed analytically in terms of certain quantities that characterize the respective molecular surface electrostatic potentials $V_S(\mathbf{r})$ [20–22]. These quantities include the most positive and the most negative values of the electrostatic potentials ($V_{S,max}$ and $V_{S,min}$, respectively). The $V_{S,max}$ of σ-holes and the $V_{S,min}$ of Lewis bases have been found to correlate with empirical measures of noncovalent interactions, namely, donating and accepting tendencies [23–25].

Since Wittig's pioneering studies on phosphonium ylides, ylides have attracted continued and continuously increasing interest. The ylides are of two types based on their relative stability. i) Non-stabilized ylides: The ylides with electron donating groups on negatively charged carbon are less stable and react faster. They also react with dioxygen. Hence the Wittig reaction with non-stabilized ylides is performed under inert atmosphere. ii) Stabilized ylides: The ylides with electron withdrawing groups adjacent to the negatively charged carbon are more stable. These are usually stabilized by conjugation (Scheme 1).

J. Ji · Y. Zeng (✉) · X. Zhang · S. Zheng · L. Meng (✉)
College of Chemistry and Material Science,
Hebei Normal University, Shijiazhuang 050024, China
e-mail: yanlizengs@163.com
e-mail: menglp@mail.hebtu.edu.cn

Scheme 1 Structures for the CH_2-XH_3(X = P, As, Sb) and CH_2-YH_2(Y = S, Se, Te) ylides

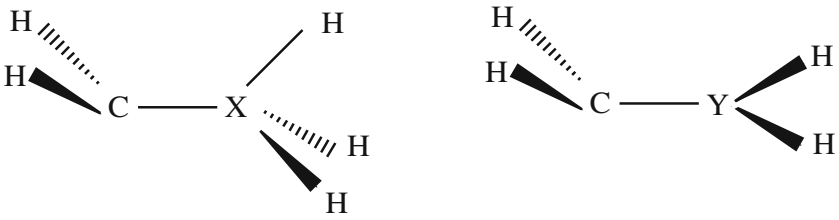

Stable ylides of sulfur, nitrogen, phosphorus, and other heteroatoms have been prepared and used in synthetic chemistry. Thus, they play important roles in promoting the progress of physical organic chemistry [26]. Since the ylides have what are considered hypervalent group V and VI atoms, it would be of interest to determine whether there are σ-holes outside pnicogen and sulfur atoms (group V and VI) along the C–P and C–S bonds in P-ylides and S-ylides. If so, then there would be interactions between σ-holes and these kinds of nucleophiles. Similar to the halogen bonding interactions, such weak interactions in ylides would be significant in several areas such as organic synthesis, crystal engineering, and design of new materials.

Computational methods

$V(\mathbf{r})$ is an effective measure for analyzing and predicting noncovalent interactions [21, 27–34]. $V(\mathbf{r})$ is the Coulombic potential felt at any point $\mathbf{r}$ in the space surrounding a charge distribution. For a system of nuclei and electrons, it is defined as

$$V(r) = \sum_A \frac{Z_A}{|R_A - r|} - \int \frac{\rho(r')dr'}{|r' - r|}, \quad (1)$$

where Z_A is the charge on nucleus A located at $\mathbf{R}_A$ and $\rho(\mathbf{r})$ is the electronic density function of the molecule. $V(\mathbf{r})$ is positive in regions where the dominant contribution is from the nuclei and negative where the dominant contribution is from electrons. $V(\mathbf{r})$ is physically observable, and can be determined experimentally by diffraction techniques [35, 36], as well as computationally.

In this work, the geometries of the monomers and the complexes were optimized with ab initio calculations using second-order Møller-Plesset perturbation theory (MP2) with a mixed basis set. The aug-cc-pVDZ-PP basis set, which uses small-core energy-consistent relativistic pseudopotentials to account for relativistic effects [37], was used for Sb and Te, whereas for all other atoms the aug-cc-pVDZ basis set was used. Corresponding frequency calculations were then carried out at the same level to confirm that the optimized geometries were true minima on the potential energy surfaces. The counterpoise procedure proposed by Boys and Bernardi [38] was used to correct the interaction energies while excluding the inherent basis set superposition error (BSSE); the same procedure was done to optimize geometries and compute frequencies. All of the aforementioned calculations were performed using the Gaussian 03 program [39].

In this work, values of $V(\mathbf{r})$ on the 0.001 and 0.01 au molecular surfaces of the molecule's electronic density were computed using Wave Function Analysis Surface analysis suite [40]. Topological analyses of electron density based on the quantum theory of atoms in molecules (QTAIM) [41, 42] were carried out with the AIMAll program [43].

Results and discussion

The σ-hole in ylides

The $V_{S,max}$ values of CH_2XH_3 (X = P, As, Sb) and CH_2–YH_2 (Y = S, Se, Te) on the 0.001 and 0.01 au contours of molecular electron density were computed, which are collected in Table 1. For the 0.01 au contour, the $V_{S,max}$ values become increasingly positive going from lighter to heavier atoms of groups V and VI, whereas there are no such tendency on the 0.001 au. Moreover, the σ-holes in the electrostatic potentials maps on the 0.01 au molecular surfaces are more obvious than those on the 0.001 au. Therefore, the $V_{S,max}$ values on the 0.01 au contour of the CH_2XH_3 (X = P, As, Sb) and CH_2–YH_2 (Y = S, Se, Te) are used to discuss in the following sections.

Figure 1 clearly shows the $V(\mathbf{r})$ of CH_2XH_3 (X = P, As, Sb) on the 0.01 au contour of molecular electron density. For CH_2–XH_3, there exists a region of positive local maximum

Table 1 Computed electrostatic potential maxima ($V_{S,max}$) on 0.001au and 0.01au molecular surfaces in the ylides

Molecule	0.01au	0.001au
CH_2PH_3	90.1	30.2
CH_2AsH_3	98.1	29.3
CH_2SbH_3	111.2	30.2
CH_2SH_2	83.9	33.7
CH_2SeH_2	86.0	29.5
CH_2TeH_2	96.0	27.8
CH_2PF_3	120.7	29.3
$CH_2P(CH_3)_3$	78.1	23.8

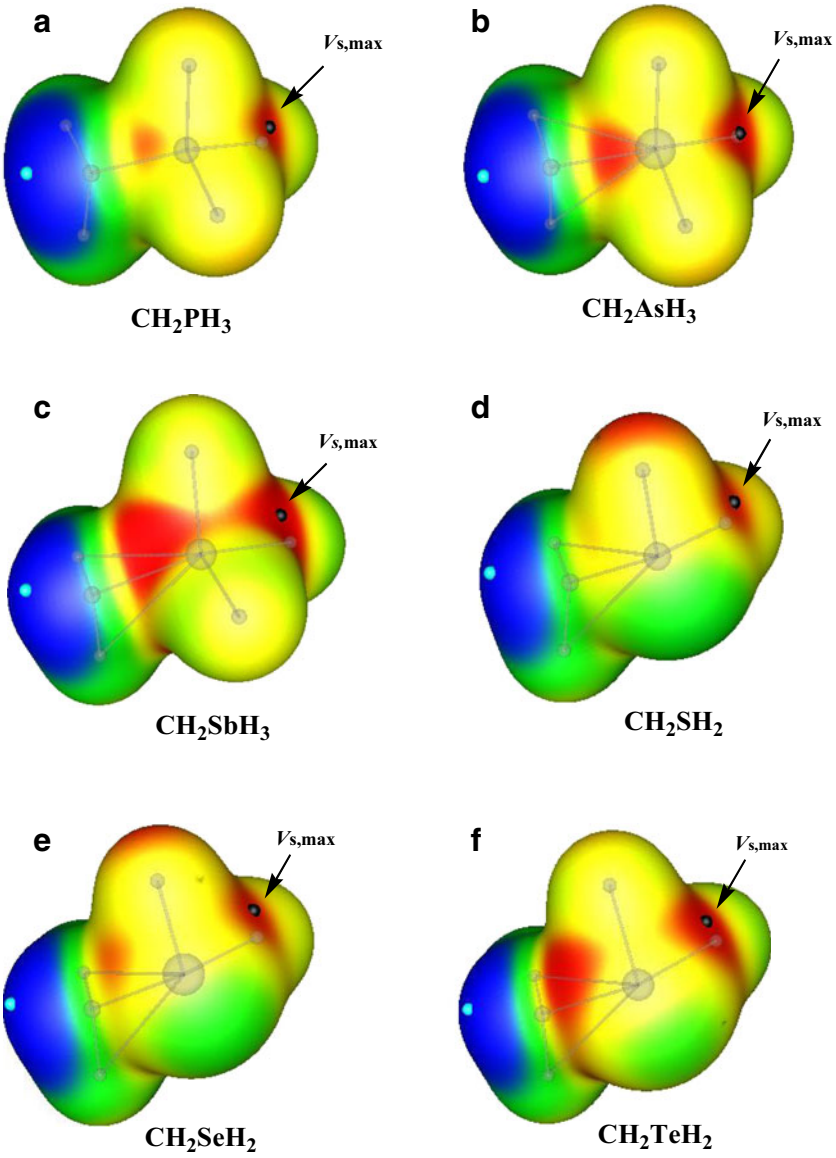

Fig. 1 Electrostatic potentials on the 0.01 au molecular surfaces: (**a**) CH_2PH_3, (**b**) CH_2AsH_3, (**c**) CH_2SbH_3, (**d**) CH_2SH_2, (**e**) CH_2SeH_2, (**f**) CH_2TeH_2. Color ranges, in kcal mol^{-1}: red, more positive than 70; yellow, 30–70; green, -20-30; blue, more negative than −20. Position of $V_{S,max}$ is indicated in black arrows

electrostatic potential in the phosphorus side on the extension of the C–X bond. Figure 2 shows the V (r) for CH_2PF_3 and $CH_2P(CH_3)_3$. –F is the electron-withdrawing group and $–CH_3$ is the electron-donating group. The figure demonstrates that the σ-hole of ylides could be affected by the substituent on phosphorus.

The σ-hole is also present in CH_2YH_2 (Y = S, Se, Te, Fig. 1). Different from CH_2XH_3 (X = P, As, Sb), the σ-hole of CH_2–YH_2 (Y = S, Se, Te) is not along the extension of the C–Y axis; instead, it is closer to the center of the two atoms of the YH_2 group, far from the lone pair of the group. The X and Y atoms in the ylides are hypervalent, and so the σ-holes on or near the extensions of C-X and C-Y bond can be compared to those on hypervalent phosphorus and sulfur in $OPCl_3$, $OPBr_3$ and $OS(CH_3)_2$, of which the most positive electrostatic potentials are along the extension of O-P and O-S bonds [9, 17].

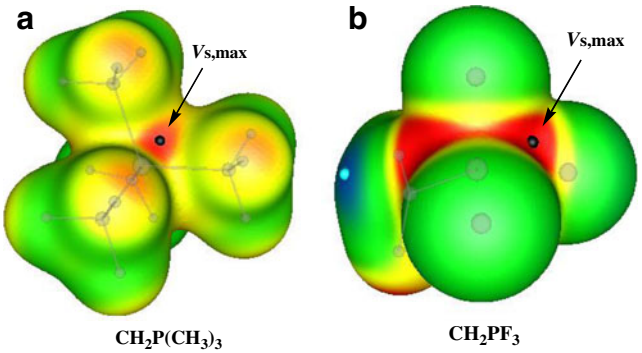

Fig. 2 Electrostatic potentials on the 0.01 au molecular surfaces: (**a**) $CH_2P(CH_3)_3$, (**b**) CH_2PF_3. Color ranges, in kcal mol^{-1}: red, more positive than 60; yellow, 30–60; green, -20-30; blue, more negative than −20. Position of $V_{S,max}$ is indicated in black arrows

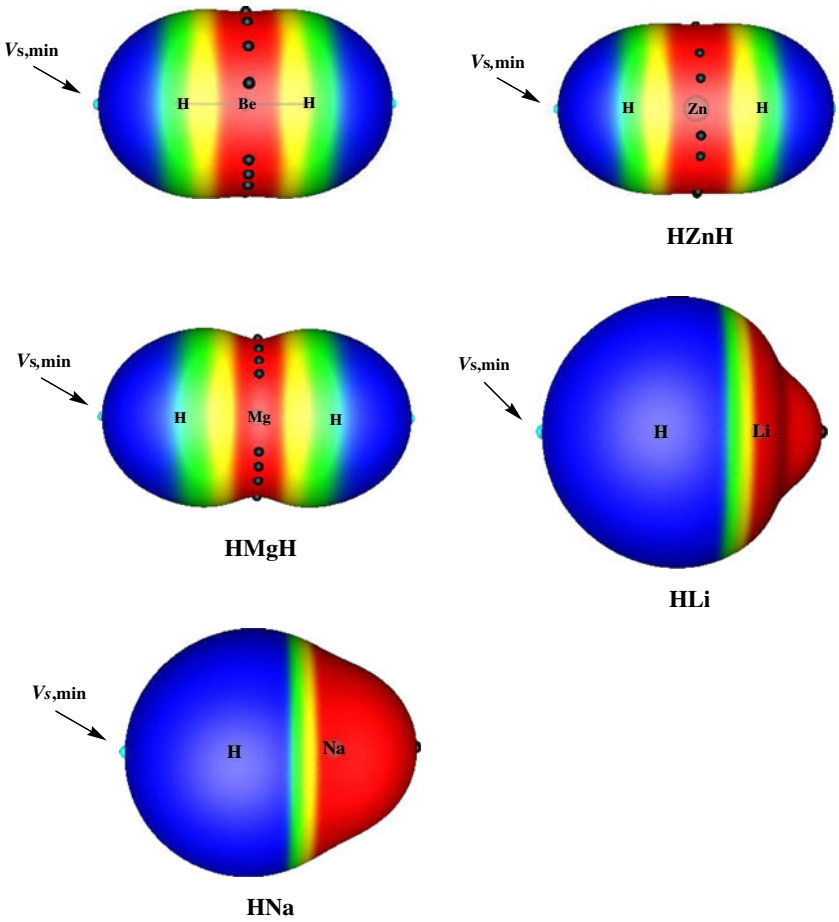

Fig. 3 Electrostatic potentials on the 0.001 au molecular surfaces of HM (M = BeH, ZnH, MgH, Li, Na). Color ranges, in kcal mol^{-1}: red, more positive than 23; yellow, 10–23; green,0-10; blue, negative. Position of $V_{S,min}$ is indicated in black arrows

The σ-hole interaction between P-ylides and HM (M = BeH, ZnH, MgH, Li, Na)

It is reasonable to expect that CH_2–XH_3 (X = P, As, Sb) and CH_2–YH_2 (Y = S, Se, Te) molecules interact noncovalently with nucleophiles approximately along the extensions of the C–X and C–Y bonds. The objective in this part is to investigate the interaction between the positive $V(\mathbf{r})$ region (σ-hole) of P-ylides and the negative $V(\mathbf{r})$ region of HM. Figure 3 shows the values of $V(\mathbf{r})$ on the 0.001 au surfaces of HM. The most negative electrostatic potentials region is outside the hydrogen atom, along the extension of the H–M bond axis. The most negative electrostatic potential ($V_{S,min}$) values of HM on the 0.001 au surfaces of the molecules are listed in Table 2.

Equilibrium geometries and interaction energy

The optimized geometry of CH_2XH_3···HM complex (X = P, As, Sb; M = BeH, ZnH, MgH, Li, Na) is displayed in Fig. 4. The hydrogen atom in HM (M = BeH, ZnH, MgH, Li, Na) is attracted to X (X = P, As, Sb) and forms the X···H bond.

Table 3 shows the interaction energies ΔE, geometrical parameters, infrared stretching frequencies, and relevant variables of the CH_2XH_3···HM complexes (X = P, As, Sb; M = BeH, ZnH, MgH, Li, Na). Values of ΔE obtained at the MP2/

Table 2 Computed electrostatic potential minimum ($V_{S,min}$) on 0.001au molecular surfaces in HM

Molecule	$V_{S,min}$ (kcal mol^{-1})
HBeH	−15.5
HZnH	−17.2
HMgH	−24.7
HLi	−53.2
HNa	−57.1

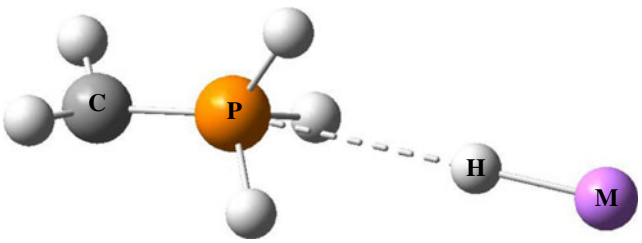

Fig. 4 The optimized geometry of the CH_2XH_3···HM (X = P, As, Sb; M = BeH, ZnH, MgH, Li, Na)

Table 3 Interaction energies, geometrical parameters, and vibrational frequencies of the complexes

	ΔE, kJ·mol^{-1}	d(X···H), Å	A(C-X···H),degree	Δd(H-M), Å	$\Delta\nu$(H-M), cm^{-1}
CH_2PH_3···HBeH	−3.17	3.210(3.00)[a]	167.3	0.001	7.04
CH_2PH_3···HZnH	−4.48	3.165 (3.00)	167.2	0.002	2.06
CH_2PH_3···HMgH	−6.67	3.146 (3.00)	167.4	0.005	7.48
CH_2PH_3···HLi	−16.57	3.031 (3.00)	168.3	0.003	21.82
CH_2PH_3···HNa	−19.21	3.023 (3.00)	168.6	0.006	32.83
CH_2AsH_3···HBeH	−3.18	3.308 (3.05)	164.8	0.002	6.22
CH_2AsH_3···HZnH	−4.49	3.256 (3.05)	164.9	0.003	0.99
CH_2AsH_3···HMgH	−6.59	3.240 (3.05)	164.9	0.005	6.03
CH_2AsH_3···HLi	−16.50	3.107 (3.05)	166.2	0.003	18.53
CH_2AsH_3···HNa	−19.32	3.092 (3.05)	166.6	0.006	30.39
CH_2SbH_3···HBeH	−2.90	3.455	162.0	0.001	6.26
CH_2SbH_3···HMgH	−6.08	3.3650	162.4	0.004	6.19
CH_2SbH_3···HLi	−15.45	3.194	163.8	0.003	18.54
CH_2SbH_3···HNa	−18.19	3.172	164.3	0.006	29.83

[a] The sums of the van der Waals distances

aug-cc-pVDZ level were corrected for BSSE and zero-point vibrational energies. The ΔE values increase in the sequence of M = BeH, ZnH, MgH, Li, Na, which is in accordance with the sequence of $V_{S,min}$ of HM in Table 2. More negative potentials of HM correspond to more stable complexes (more negative ΔE). Figure 5 displays the relationship between ΔE and $V_{S,min}$ of HM. The linear correlation coefficients are as follows: 0.9977 for CH_2PH_3···HM, 0.9971 for CH_2AsH_3···HM, and 0.9971 for CH_2SbH_3···HM. These relationships indicate that the strength of the X···H interaction is greatly affected by the $V_{S,min}$ of HM.

The X···H distances d(X···H) are listed in Table 3, it may be compared against the sums of the van der Waals radii of the respective atoms, which can give a rough indication of the maximum separation for the nonvalent interaction. In our study, d(X···H) denotes the distance between the X atom (X = P, As, Sb) of CH_2XH_3 and the hydrogen atom of HM. The d(X···H) values are somewhat greater than the sums of the van der Waals radii, indicating that the CH_2XH_3···HM are weakly bound complexes.

The interaction angles A(C–X···H) range from 162.0° to 168.6°, and are all close to 180°. These angles therefore suggest that the hydrogen atom of HM is near the extension of the C–X bond to the X atom that produced the σ-hole. The closeness of such angles to 180° is one of the characteristic features of the σ-hole interaction. Their deviation from 180° is due to the effects of the CH_2 group of CH_2XH_3 [13, 17, 44, 45].

The H–M bonds in the complexes are longer than those in the respective monomers. The H–M bond-stretching frequencies in the complexes are shifted to higher values compared

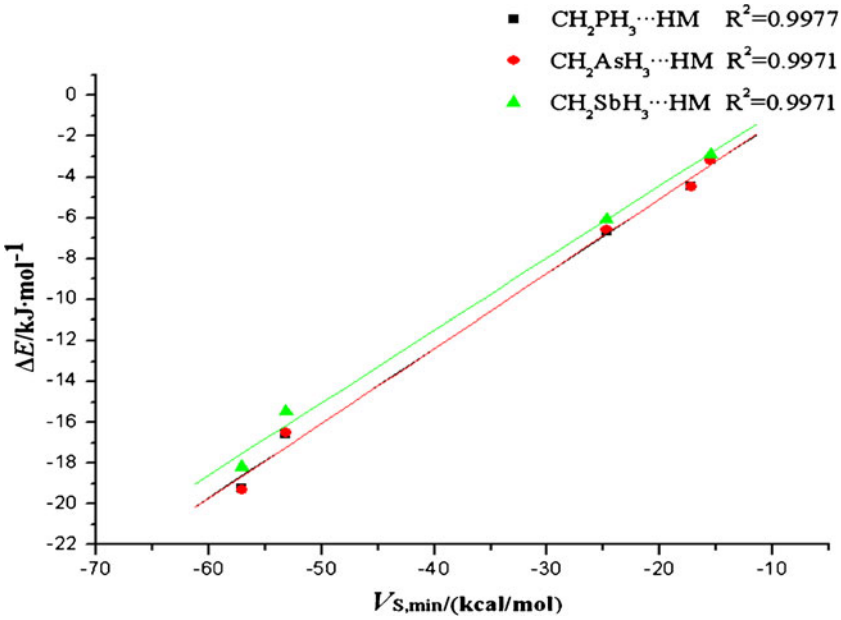

Fig. 5 Linear relationships between the interaction energies ΔE and $V_{S,min}$ of HM. Linear relationships between the H···X distances and $V_{S,min}$ of HM

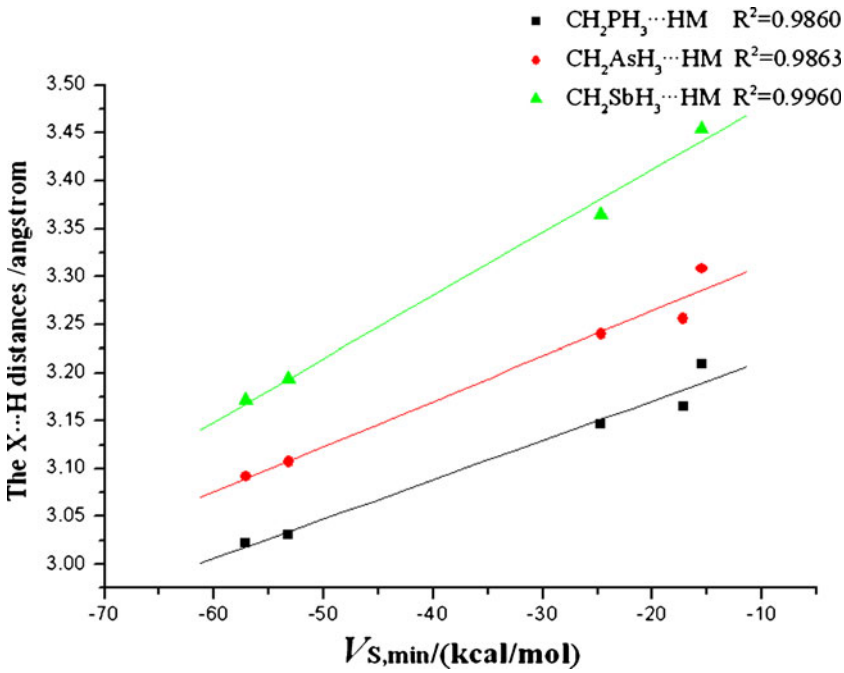

Fig. 6 Linear relationships between the H···X distances and $V_{S,min}$ of HM

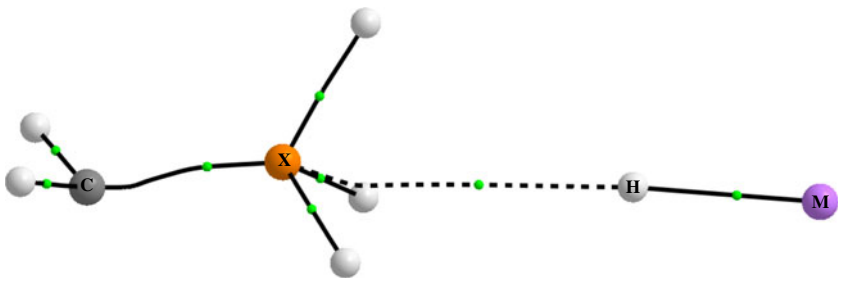

Fig. 7 Molecular graphs of CH_2XH_3···HM (X = P, As, Sb; M = Li, Na, MgH, ZnH, BeH)

Table 4 Topological and energy properties at the X···H bond critical points of the complexes (all values in a.u.)

	ρ_b	λ_1	λ_2	λ_3	$\nabla^2\rho_b$	G_b	V_b	H_b	$-G_b/V_b$
CH_2PH_3···HBeH	0.0039	−0.0010	−0.0006	0.0155	0.0139	0.0027	−0.0018	0.0008	1.4475
CH_2PH_3···HZnH	0.0045	−0.0010	−0.0006	0.0176	0.0160	0.0031	−0.0021	0.0009	1.4455
CH_2PH_3···HMgH	0.0049	−0.0013	−0.0005	0.0187	0.0168	0.0033	−0.0023	0.0010	1.4134
CH_2PH_3···HLi	0.0065	−0.0017	−0.0004	0.0238	0.0217	0.0042	−0.0030	0.0012	1.3937
CH_2PH_3···HNa	0.0068	−0.0016	−0.0005	0.0244	0.0223	0.0044	−0.0032	0.0012	1.3811
CH_2AsH_3···HBeH	0.0037	−0.0011	−0.0007	0.0141	0.0123	0.0024	−0.0016	0.0007	1.4437
CH_2AsH_3···HZnH	0.0043	−0.0012	−0.0007	0.0162	0.0143	0.0027	−0.0019	0.0008	1.4371
CH_2AsH_3···HMgH	0.0047	−0.0015	−0.0006	0.0171	0.0150	0.0029	−0.0021	0.0008	1.4030
CH_2AsH_3···HLi	0.0063	−0.0019	−0.0008	0.0224	0.0196	0.0039	−0.0028	0.0010	1.3669
CH_2AsH_3···HNa	0.0067	−0.0019	−0.0009	0.0231	0.0203	0.0040	−0.0030	0.0010	1.3500
CH_2SbH_3···HBeH	0.0034	−0.0010	−0.0007	0.0126	0.0109	0.0021	−0.0014	0.0007	1.4644
CH_2SbH_3···HMgH	0.0045	−0.0013	−0.0008	0.0155	0.0134	0.0026	−0.0019	0.0007	1.3760
CH_2SbH_3···HLi	0.0064	−0.0020	−0.0014	0.0213	0.0179	0.0037	−0.0029	0.0008	1.2839
CH_2SbH_3···HNa	0.0069	−0.0021	−0.0016	0.0222	0.0186	0.0038	−0.0030	0.0008	1.2648

with those in the respective monomers. These are abnormal blue shifts of the H–M bond-stretching frequency, which are not consistent with the H–M bond elongations [46].

Figure 6 displays highly linear relationships between the d(X···H) and $V_{S,min}$ values of HM in Table 2. The linear correlation coefficients are as follows: 0.9860 for CH_2PH_3···HM, 0.9863 for CH_2AsH_3···HM, and 0.9960 for CH_2SbH_3···HM. These values indicate that more negative potentials of HM correspond to lower d(X···H) values and more stable complexes.

QTAIM analyses

Many studies have indicated that the QTAIM theory is very useful for studying the properties of conventional and unconventional interactions [47–49]. By means of topological analysis, features such as critical points and paths of maximum electron density (atomic interaction lines) can be studied, as AIM provides a molecular graph representing the bonding interactions [50].

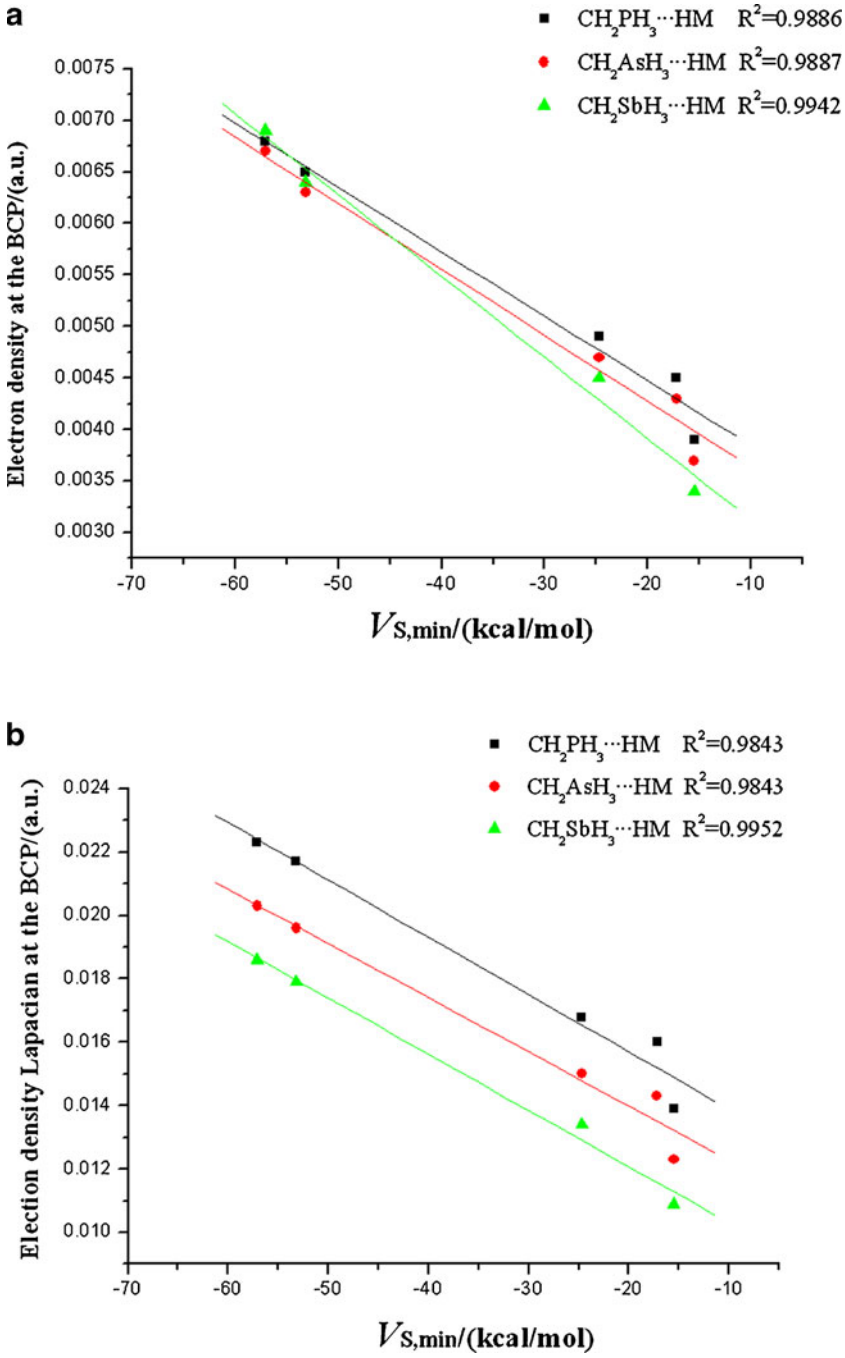

Fig. 8 Linear relationships between topological properties at the BCP and the $V_{s,min}$ of HM. (**a**) Electron density ρ_b and the $V_{s,min}$ of HM, (**b**) Electron density Laplacian $\nabla^2\rho_b$ and $V_{S,min}$ of HM

Figure 7 shows the molecular graph of the $CH_2XH_3\cdots HM$ complex (X = P, As, Sb). The bond critical point (BCP) between X(1) and H(10) indicates the formation of the X(1)···H(10) bond. The electron density ρ_b at the X-H BCP, the Laplacian of the electron density $\nabla^2\rho_b$, and the total electron energy density H_b for each complex are presented in Table 4.

According to the topological analysis of electronic density distribution in the AIM theory, ρ_b is used to describe the strength of a bond. In general, the larger the value of ρ_b, the stronger the bond [41]. A negative value of $\nabla^2\rho_b$ indicates that there is a shared interaction (as in a covalent bond), whereas a positive value indicates the interaction in closed-shell systems, that is, ionic interactions, van der Waals forces, or hydrogen bonding [41]. The values of ρ_b of $CH_2XH_3\cdots HM$ increases in the sequence of M = BeH, ZnH, MgH, Li, Na. This trend is in accordance with the sequence of $V_{S,min}$ values of HM in Table 2. Figure 8(a) presents the linear relationships between ρ_b and $V_{S,min}$ of HM. The linear correlation coefficients are as follows: 0.9886 for $CH_2PH_3\cdots HM$, 0.9887 for $CH_2AsH_3\cdots HM$, and 0.9942 for $CH_2SbH_3\cdots HM$. These values indicate that more negative $V(\mathbf{r})$ values of HM correspond to larger ρ_b values and stronger X(1)···H(10) interaction. Figure 8(b) presents the linear relationships between $\nabla^2\rho_b$ and $V_{S,min}$ of HM, for which the correlation coefficients are as follows: 0.9843 for $CH_2PH_3\cdots HM$, 0.9843 for $CH_2AsH_3\cdots HM$, and 0.9952 for $CH_2SbH_3\cdots HM$. These results suggest that more negative values of HM correspond to more positive $\nabla^2\rho_b$ values and a more electrostatic character of the X(1)···H(10) interaction. These relations show that the topological properties (ρ_b, $\nabla^2\rho_b$) at the BCPs are correlated with $V(\mathbf{r})$.

The kinetic electron energy density G_b, the potential electron energy density V_b, the electron energy density H_b, and $-G_b/V_b$ at the X(1)···H(10) BCPs are also listed in Table 4. Parameters derived from the Bader theory indicate the type of interaction. Values of $\nabla^2\rho_b$ and H_b indicate the nature of the interaction. In particular, if $\nabla^2\rho_b$ is positive but H_b is negative, then the interaction is partly covalent in nature [51, 52]. The value of $-G_b/V_b$ indicate the regions corresponding to covalent or noncovalent interactions, as it represents the balance between the positive value of G_b and the negative value of V_b. If $-G_b/V_b$ is greater than 1, then the interaction is noncovalent; if it is between 0.5 and 1, then the interaction is partly covalent; and when it is less than 0.5, then the interaction is a shared covalent one. The data in Table 4 show that the X(1)···H(10) interactions display the characteristics of closed-shell noncovalent interactions.

Figure 9 shows the relationship of G_b and V_b with $V_{S,min}$ of HM. The trends indicate that more negative values of $V_{S,min}$ of HM are associated with smaller values of G_b and larger values of V_b. These relations show that the energy properties (G_b, V_b) at the BCPs are also correlated with $V(\mathbf{r})$.

Conclusions

(1) Positive $V(\mathbf{r})$ values have been found on the outer surfaces of group VA and VIA atoms of the ylides CH_2XH_3 (X = P, As, Sb) and CH_2YH_2 (Y = S, Se, Te), approximately along the extensions of C–X and C–Y bonds, respectively. The origins of the $V(\mathbf{r})$ values can be explained in terms of the σ-hole concept.

(2) CH_2XH_3 (X = P, As, Sb) ylide molecules can interact noncovalently with nucleophiles HM (M = Li, Na, BeH, MgH, ZnH) approximately along the extensions of the C–X and. The geometries of the complexes are determined by the $V_{S,max}$ of the σ-hole region and the $V_{S,min}$ of the hydrides.

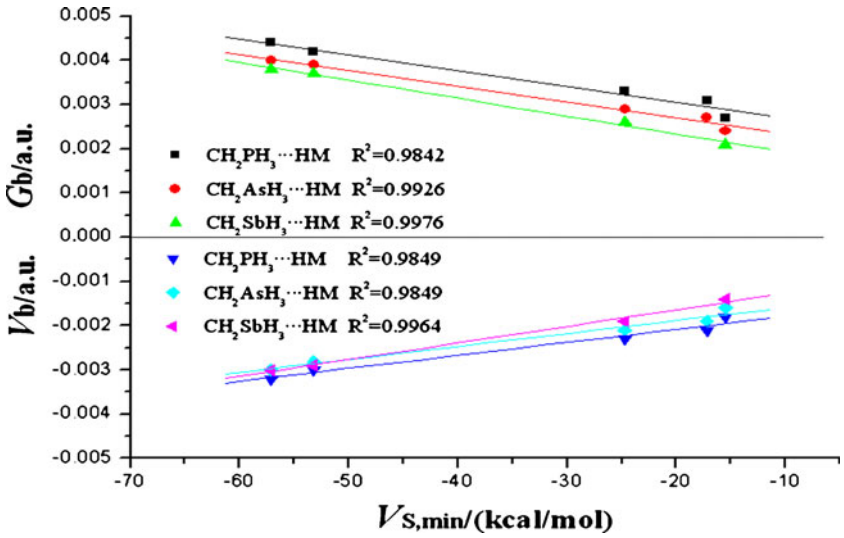

Fig. 9 Linear relationships between local energy densities (G_b and V_b) at the BCP of the H···X bond and $V_{S,min}$ of HM

(3) The X(1)···H(10) interactions in the CH_2XH_3···HM complexes (X = P, As, Sb; M = HM) manifest the characteristics of closed-shell and noncovalent interactions.
(4) The interaction energies, interaction distances, topological properties (ρ_b, $\nabla^2\rho_b$) and energy properties (G_b, V_b) at the X(1)···H(10) BCPs are all correlated with the $V_{S,min}$ values of HM, indicating that electrostatic interactions play an important role in weak X···H interactions in CH_2XH_3···HM complexes.
(5) Similar to halogen bonding interactions, weak interactions involving ylides may be significant in several areas such as organic synthesis, crystal engineering, and design of new materials.

Acknowledgments Thanks for International Science Editing to edit this paper. This project was supported by the National Natural Science Foundation of China (Contract Nos.: 21371045, 21102033, 21171047, 21073051), the Natural Science Foundation of Hebei Province (Contract No.: B2011205058), and the Education Department Foundation of Hebei Province (ZH2012106, ZD2010126).

References

1. Buckingham AD, Fowler PW, Hutson JM (1988) Chem Rev 88:963–988
2. Chałasiński G, Szcze śniak MM (2000) Chem Rev 100:4227–4252
3. Wormer PES, van der Avoird A (2000) Chem Rev 100:4109–4144
4. Philp D, Stoddart JF (1996) Angew Chem Int Ed Engl 35:1154–1196
5. Klos J, Szcze śniak MM, Chałasiński G (2004) Int Rev Phys Chem 23:541–571
6. Saalfrank RW, Maid H, Scheurer A (2008) Angew Chem Int Ed Engl 47:8794–8824
7. Llanes-Pallas A, Palma CA, Piot L et al. (2009) J Am Chem Soc 131:509–520
8. Clark T, Hennemann M, Murray JS et al. (2007) J Mol Model 13:291–296
9. Politzer P, Murray JS (2013) Chemphyschem 14:278–294
10. Politzer P, Murray JS, Clark T (2010) Phys Chem Chem Phys 12:7748–7757
11. Auffinger P, Hays FA, Westhof E et al. (2004) Proc Natl Acad Sci U S A 101:16789–16794
12. Politzer P, Lane P, Concha MC et al. (2007) J Mol Model 13:305–311
13. Murray JS, Lane P, Politzer P (2007) Int J Quantum Chem 107:2286–2292
14. Murray JS, Concha MC, Lane P et al. (2008) J Mol Model 14:699–704
15. Solimannejad M, Ramezani V, Trujillo C et al. (2012) J Phys Chem A 116:5199–5206
16. Murray JS, Lane P, Clark T et al. (2012) J Mol Model 18:541–548
17. Murray JS, Lane P, Politzer P (2009) J Mol Model 15:723–729
18. Clark T, Murray JS, Lane P et al. (2008) J Mol Model 14:689–697
19. Politzer P, Murray JS, Clark T (2013) Phys Chem Chem Phys 15:11178–11189
20. Murray JS, Politzer P (1998) J Mol Struct (THEOCHEM) 425:107–114
21. Politzer P, Murray JS (1999) Trends Chem Phys 7:157–165
22. Politzer P, Murray JS (2001) Fluid Phase Equilib 185:129–137
23. Hagelin H, Murray JS, Politzer P et al. (1995) Can J Chem 73:483–488
24. Zeng Y, Zhang X, Li X et al. (2011) Chemphyschem 12:1080–1087
25. Zeng Y, Zhu M, Li X et al. (2012) J Comput Chem 33:1321–1327
26. Johnson AW (1966) Ylid chemistry. Academic Press, New York
27. Scrocco E, Tomasi J (1973) The electrostatic molecular potential as a tool for the interpretation of molecular properties. Springer, Berlin
28. Politzer P, Daiker KC (1981) In: Deb BM (ed) The force concept in chemistry. Reinhold, New York
29. Politzer P, Laurence PR, Jayasuriya K (1985) Environ Health Perspect 61:191–202
30. Naray-Szabo G, Ferenczy GG (1995) Chem Rev 95:829–847
31. Murray JS, Politzer P (2011) WIREs Comput Mol Sci 1:153–163
32. Murray JS, Politzer P (2009) Croat Chem Acta 82:267–275
33. Politzer P, Murray JS (2002) Theor Chim Acta 108:134–142
34. Politzer P, Murray JS (1991) Reviews in computational chemistry. VCH, New York
35. Stewart RF (1979) Chem Phys Lett 65:335–342
36. Politzer P, Truhlar DG (1981) Chemical applications of atomic and molecular electrostatic potentials. Plenum, New York
37. Peterson KA, Figgen D, Goll E et al. (2003) J Chem Phys 119:11113
38. Boys SF, Bernardi F (1970) Mol Phys 19:553–566
39. Frisch MJ, Trucks GW, Schlegel HB et al. (2004) Gaussian 03. Revision D.01 ed. Gaussian, Inc., Wallingford
40. Bulat FA, Toro-Labbe A, Brinck T et al. (2010) J Mol Model 16:1679–1691
41. Bader RFW (1990) Atoms in molecules: A quantum theory. Oxford University Press, Oxford
42. Popelier PLA (2000) Atoms in molecules: an introduction. Pearson, Essex
43. Keith TA (2012) AIMALL. version 13.02.26 ed. USA
44. Murray JS, Lane P, Clark T et al. (2007) J Mol Model 13:1033–1038
45. Politzer P, Murray JS, Concha MC (2008) J Mol Model 14:659–665
46. Zeng Y, Li X, Zhang X et al. (2011) J Mol Model 17:2907–2918
47. Hobza P, Havlas Z (2000) Chem Rev 100:4253–4264
48. Lapointe SM, Farrag S, Bohorquez HJ et al. (2009) J Phys Chem B 113:10957–10964
49. Grabowski SJ (2011) Chem Rev 111:2597–2625
50. Zeng Y, Zhang X, Li X et al. (2010) Int J Quantum Chem 11:3725–3740
51. Cremer D, Kraka E (1984) Angew Chem Int Ed Engl 23:627–628
52. Bone RGA, Bader RFW (1996) J Phys Chem 100:10892–10911